CHIN.PHYS.LETT. Vol. 32, No. 3 (2015) 037501. DOI: 10.1088/0256-307X/32/3/037501

Fabrication and Characterization of Fe-doped In2O3 Dilute Magnetic Semiconducting Nanowires

Junran Zhang,[1] Xuefeng Wang,[1,a)] Zhongxia Wei,[2] Zhenyao Wu,[1] Meng Tang,[1] Wei Niu,[1] Ming Gao,[1] Zhanpeng Lv,[1] Wenqing Liu[3], Fengqi Song,[2] Jun Du,[2] Liang He,[1] Rong Zhang,[1] and Yongbing Xu[1,3,a)]

[1]National Laboratory of Solid State Microstructures, Collaborative Innovation Center of Advanced Microstructures, School of Electronic Science and Engineering, Nanjing University, Nanjing 210093, China

[2]National Laboratory of Solid State Microstructures, Collaborative Innovation Center of Advanced Microstructures, Department of Physics, Nanjing University, Nanjing 210093, China

3 York-Nanjing International Center of Spintronics (YNICS), Department of Electronics, The University of York, YO10 3DD, UK

ABSTRACT Fe-doped In_2O_3 dilute magnetic semiconducting nanowires were fabricated on Au-deposited Si substrate by chemical vapor deposition technique. It is confirmed, by energy dispersive x-ray spectroscopy (EDS), x-ray photoelectron spectroscopy (XPS) and Raman spectroscopy, that Fe has been successfully doped into lattices of In_2O_3 nanowires. The EDS measurements reveal a large amount of oxygen vacancies existing in the Fe-doped In_2O_3 nanowires. The Fe dopant exists as the mixture of Fe^{2+} and Fe^{3+} as revealed by the XPS. The origin of room-temperature ferromagnetism in the Fe-doped In_2O_3 nanowires is explained by the bound magnetic polaron model.

KEYWORDS: Fe-doping, In_2O_3 nanowires, ferromagnetism

PACS: 75.10.-b; 81.15.Gh; 06.60.-c

[a)] Authors to whom correspondence should be addressed. Electronic addresses: xfwang@nju.edu.cn and ybxu@nju.edu.cn.

Dilute magnetic semiconductors (DMSs) are promising supporting materials for future spintronic devices, utilizing both spin and charge degrees of freedom.[1] Among many promising materials, wide-band-gap oxide semiconductors, such as ZnO,[2] TiO_2,[3] SnO_2,[4] In_2O_3,[5] and also Ga_2O_3,[6] are especially intriguing host materials for DMSs due to their transparent spintronic applications. In_2O_3 with a wide direct band gap of ~3.6 eV has attracted much attention in recent years, owing to its distinctive optical, chemical, and electronic properties. It has great potential for the applications in solar cells,[7] field-emission displays,[8] lithium-ion batteries,[9] nanoscale biosensors,[10] gas sensors,[11] optoelectronics,[12] and photocatalysis.[13] It was reported that In_2O_3-based DMSs doped with Fe,[14] Co,[15] Ni,[16] Nd,[17] Mn,[18] Cr,[19] and V[20] exhibited strong room-temperature ferromagnetism (RTFM). Among the DMSs, the Fe-doped In_2O_3 is most attractive because of its high optical transparency, electric conductivity, and high Curie temperature.[14] In addition, the electron charge carriers in Fe-doped In_2O_3 are spin polarized as it is required for spin injection in the practical applications.[21] Furthermore, due to the relatively high solubility of Fe in In_2O_3 (up to 20 at.%), Fe-doped In_2O_3 is a suitable system to study the mechanism of impurity ferromagnetism in DMSs for the potential application in spintronics.[21]

Many investigations on the synthesis methodology and properties about different dimensions of In_2O_3 having been reported, such as bulk single crystals,[22] thin films,[23] porous sheets,[24] nanowires,[5] nanocubes,[25] and so on. However, pioneering studies of Fe-doped In_2O_3 have mainly focused on the bulk,[26] thin films,[27] and nanocrystals,[14] whereas reports on Fe-doped In_2O_3 nanowires still remain few. Since the performance of some applications is expected to be improved by lowering the dimension or increasing the surface-to-volume ratio, one-dimensional Fe-doped In_2O_3 nanowires have obvious advantages. In addition, it has been reported that the spin lifetime (spin relaxation time) in nanowires is much longer than that in bulk,[28, 29] thus In_2O_3-based DMS nanowires are required for exploiting the advantages offered by the spin.

The origins of ferromagnetism in DMSs include intrinsic carriers,[30, 31] structural defects,[32] mixed valence state,[33] dopant-defect complexes,[34] and the presence of secondary

phases.[35] While the Fe-doped In_2O_3 thin films[21] and nanocrystals[14] have been studied rather extensively, the mechanism of RTFM in Fe-doped In_2O_3 nanowires is not clear, and it is still an open issue whether the magnetism is similar to that of Fe-doped In_2O_3 thin films.

In this work, we firstly fabricated Fe-doped In_2O_3 nanowires by an Au-catalyzed chemical vapor deposition (CVD) method. A mixture of high-purity In_2O_3 and C, with nominal atomic ratio of 1:2, was put in a cleaned quartz boat, and the other quartz boat held high-purity $Fe(OH)_3$. Then the furnace was slowly heated to 1000 ºC and kept at this temperature for 1 h with the mixed high-purity gas of O_2 and Ar flowing. And as-prepared samples were annealed at 600 ºC for 12 h in high-purity O_2. Fe is confirmed to be incorporated into In_2O_3 nanowires by energy dispersive x-ray spectroscopy (EDS), x-ray photoelectron spectroscopy (XPS), and Raman spectroscopy measurements. The room temperature magnetic properties of In_2O_3 and Fe-doped In_2O_3 nanowires were measured by vibrating sample magnetometer.

Figure 1 shows the typical SEM images of In_2O_3 and Fe-doped In_2O_3 nanowires. The diameter of In_2O_3 nanowires is about 100-500 nm, and the length is about 20-50 μm, while Fe-doped In_2O_3 nanowires are 500-900 nm in diameter and 30-70 μm in length. One can see that the diameter and length of In_2O_3 nanowires become larger upon Fe doping. This can be explained in term of the more favorable crystal growth caused by high solubility of Fe in In_2O_3 nanowires.

In order to confirm that whether Fe is doped into In_2O_3 nanowires successfully or not, we carried out the EDS analysis for Fe-doped In_2O_3 nanowire as shown in Fig. 2. Fig. 2(a) plots the EDS spectrum of In_2O_3 nanowires. From the result of Fig. 2(b), we can see that 2.37 at.% Fe was doped into In_2O_3 nanowires. The ratio of O and In is about 54.43 versus 44.71, which is smaller than the standard ratio of 3:2. This implies that oxygen vacancies (V_o) exist in Fe-doped In_2O_3 nanowires, which is one of factors inducing the RTFM, as discussed later. The elemental mapping shown in Fig. 2(a) and Fig. 2(b) reveals the relatively uniform distribution of In, O, and Fe in samples.

To investigate the chemical binding states of the Fe dopant and In in the nanowires, XPS

measurements were performed for Fe-doped In_2O_3 nanowires after removing a thin layer via electron bombardment to avoid surface impurity as shown in Fig. 3. The binding energies of sample were corrected using the C 1s value of 284.5 eV. One can see the XPS peaks of C, O, In, and Fe in the XPS survey spectrum [Fig. 3(a)], and the peaks of Fe are very weak due to the low concentration. Fig. 3(b) shows the high-resolution XPS spectrum for In 3d, where In $3d_{5/2}$ and $3d_{3/2}$ were observed at ~443.75 and ~451.25 eV, respectively, indicating that elemental In exists in 3+ valence state, corresponding to the formation of the In_2O_3 phase. The O 1s peak with the binding energy of ~529.25 eV reveals that O is O^{2-} state as shown in Fig. 3(c). Fig. 3(d) shows the high-resolution Fe 2p spectrum of Fe-doped In_2O_3 nanowires. For the sample, the observed XPS peaks can be Gaussian divided into Fe^{2+} peaks and Fe^{3+} peaks. The Fe^{2+}/Fe^{3+} atomic ratio is about 1:3, according to the ratio of the areas for the Fe^{2+} and Fe^{3+} peaks. When the V_o sits close to the Fe site, the remaining 4s electrons lead to a Fe^{2+} state via charge transfer. It is worth mentioning that a characteristic shake-up satellite peak for Fe^{3+} species is clearly visible at the binding energy of 712.5 eV, which indicates that the mixture of Fe^{2+} and Fe^{3+} does not originate from the formation of Fe_3O_4 since the binding energy of Fe $2p_{3/2}$ in Fe_3O_4 does not have a satellite peak.[36] Hence, we can make a further confirmation that Fe indeed exists in In_2O_3 as the mixture of Fe^{2+} and Fe^{3+}.

The Raman spectra of In_2O_3 and Fe-doped In_2O_3 nanowires were recorded at room temperature using a confocal laser Raman spectrometer and the results are shown in Fig. 4. In the range of 100-700 cm^{-1}, six scattering peaks (110, 131, 305, 364, 494, and 629 cm^{-1}) are observed, and their positions are approximately in agreement with those of previously reported body-centered cubic In_2O_3 Raman spectra.[37] The peak at 131 cm^{-1} is assigned to the In-O vibration of [InO_6] structural units; the peak at 305 cm^{-1} is assigned to the bending vibration of δ-[InO_6] octahedrons; the other two peaks 497 and 630 cm^{-1} are attributed to the stretching vibrations of the same ν-[InO_6] octahedrons; whereas the 367 cm^{-1} is assigned to the stretching vibrations of the In-O-In bonds.[38] We can see that the incorporation of Fe in In_2O_3 leads to the peaks' position shift towards the lower frequency as compared with pure In_2O_3,[37, 39] which is attributed to the strain induced by Fe^{2+} and Fe^{3+} in the sample.

Figure 5 shows the plots of magnetization vs. magnetic field measured at room

temperature for the as-grown and annealed samples (In_2O_3 and Fe-doped In_2O_3 nanowires) with subtracting the magnetic contribution of substrate as showing in the inset. All the four samples show well-defined ferromagnetic behavior in spite of weak magnetization caused by low doping content. Saturated magnetizations (M_s) of as-grown (~9.72×10^{-3} emu/g) and annealed (~7.14×10^{-3} emu/g) Fe-doped In_2O_3 are all much larger than as-grown and annealed pure In_2O_3 (both is ~1×10^{-3} emu/g). After annealing, M_s and coercive fields (H_c) (from 140 to 100 Oe) of Fe-doped In_2O_3 decreased.

Here we discuss in details the origin of the magnetic behavior in Fe-doped In_2O_3 nanowires. Based on the above EDS and XPS results, it is reasonable to suggest that there are a lot of V_o in samples, and V_o bring about distortion of the nearby lattice and redistribution of the charges around. Since Fe^{2+} ions were observed by XPS in the nanowires, therefore, In^{3+}-(↓)-Fe^{2+} complexes are formed near the V_o, where ↓ denotes an V_o which traps an electron with the spin moment ↓ relative to the spin moment ↑ of the Fe^{2+}. Also, for the Fe ions far from the V_o, they still exist in the In^{3+}-V_o-Fe^{3+} complexes form. The trapped electron (↓) in the In^{3+}-(↓)-Fe^{2+} complex can be regarded as an F-center and occupies an hydrogenic-like orbit with a radius $r=k(m/m^*)a_0$ (where k is the high frequency dielectric constant, m is the electron mass, m^* is the effective mass of the electron, and a_0 is the Bohr radius).[40] Within the radius r, the orbit of the trapped electron overlaps the localized unfilled 3*d* orbitals of the Fe^{3+} in the In^{3+}-V_o-Fe^{3+} complexes, and a fraction of electrons hop between the overlapped orbitals, leading to a local ferromagnetic ordering just like a bound magnetic polaron (BMP). The BMPs tend to overlap and create a spin-split impurity band at the Fermi level in the forbidden band, hence leading to the RTFM.[2] After annealing, the decrease in M_s and H_c for Fe-doped In_2O_3 caused by decreasing V_o further illustrates the contribution of V_o to the ferromagnetic behavior, which is corresponding to the theoretical calculations in Fe-doped In_2O_3 by Guan *et al*.[41] and experimental results in Fe-doped In_2O_3 thin films and Cu-doped In_2O_3 nanowires by An *et al*.[42] and Zou *et al*.,[32] respectively.

In conclusion, we have successfully synthetized the Fe-doped In_2O_3 nanowires by a CVD route. 2.37 at.% Fe was doped into In_2O_3 nanowire by EDS analysis. XPS spectrum reveals that Fe exists in In_2O_3 as the mixture of Fe^{2+} and Fe^{3+}. The Raman peaks of In_2O_3 and

Fe-doped In_2O_3 illustrate both of them are cubic bixbyite structure and incorporation of Fe in In_2O_3 leads to the peaks' position shift. The RTFM of Fe-doped In_2O_3 nanowires is suggested to be originated from overlap of spin-split impurity band at the Fermi level by BMPs in the forbidden band as described by the framework of the BMP model.

This work was supported by the National Key Projects for Basic Research of China (2014CB921101, 2014CB921103, and 2013CB922103), the National Natural Science Foundation of China (11274003, 61176088, and 61274102), the Program for the New Century Excellent Talents in University (NCET-11-0240), the PAPD project, and the Fundamental Research Funds for the Central Universities.

References

[1]. Wolf S A, Awschalom D D, Buhrman R A, Daughton J M, Von Molnar S, Roukes M L, Chtchelkanova A Y and Treger D M 2001 *Science* **294** 1488

[2]. Wang X F, Xu J B, Zhang B, Yu H G, Wang J, Zhang X, Yu J G and Li Q 2006 *Adv. Mater*. **18** 2476

[3]. Toyosaki H, Fukumura T, Yamada Y, Nakajima K, Chikyow T, Hasegawa T, Koinuma H and Kawasaki M 2004 *Nature Mater*. **3** 221

[4]. Fitzgerald C, Venkatesan M, Dorneles L, Gunning R, Stamenov P, Coey J M D, Stampe P, Kennedy R, Moreira E and Sias U 2006 *Phys. Rev. B* **74** 115307

[5]. Shen Y, Turner S, Yang P, Van Tendeloo G, Lebedev O I and Wu T 2014 *Nano Lett*. **14** 4342

[6]. Onuma T, Fujioka S, Yamaguchi T, Higashiwaki M, Sasaki K, Masui T and Honda T 2013 *Appl. Phys. Lett*. **103** 041910

[7]. Mori S and Asano A 2010 *J. Phys. Chem. C* **114** 13113

[8]. Wang B, Zhou Z, Wu H Y and Zhu L F 2014 *Nanoscale Res. Lett*. **9** 111

[9]. Osiak M, Khunsin W, Armstrong E, Kennedy T, Torres C M, Ryan K M and O'Dwyer C 2013 *Nanotechnology* **24** 065401

[10]. Li C, Curreli M, Lin H, Lei B, Ishikawa F N, Datar R, Cote R J, Thompson M E, and Zhou C W 2005 *J. Am. Chem. Soc*. **127** 12484

[11]. Zang W, Nie Y, Zhu D, Deng P, Xing L and Xue X 2014 *J. Phys. Chem. C* **118** 9209

[12]. Koida T, Shibata H, Kondo M, Tsutsumi K, Sakaguchi A, Suzuki M and Fujiwara H 2012 *J. Appl. Phys*. **111** 063721

[13]. Tseng W J, Tseng T T, Wu H M, Her Y C, Yang T J and Gouma P 2013 *J. Am. Ceram.*

Soc. **96** 719

[14]. Yan S, Qiao W, Zhong W, Au C T and Dou Y 2014 *Appl*. *Phys*. *Lett*. **104** 062404

[15]. An Y, Yang D, Ma G, Zhu Y, Wang S, Wu Z and Liu J 2014 *J*. *Phys*. *Chem*. *C* **118** 10448

[16]. Hong N H, Sakai J, Huong N T and Brizé V 2005 *Appl*. *Phys*. *Lett*. **87** 102505

[17]. Xing G Z, Yi J B, Yan F, Wu T and Li S 2014 *Appl*. *Phys*. *Lett*. **104** 202411

[18]. An Y, Wang S, Duan L, Liu J and Wu Z 2013 *Appl*. *Phys*. *Lett*. **102** 212411

[19]. Philip J, Punnoose A, Kim B I, Reddy K M, Layne S, Holmes J O, Satpati B, Leclair P R, Santos T S and Moodera J S 2006 *Nature Mater*. **5** 298

[20]. Gupta A, Cao H T, Parekh K, and Rao K V 2007 *J*. *Appl*. *Phys*. **101** 09N513

[21]. Kim H, Osofsky M, Auyeung R C Y and Piqué A 2012 *Appl*. *Phys*. *Lett*. **100** 142403

[22]. Scherer V, Janowitz C, Krapf A, Dwelk H, Braun D and Manzke R 2012 *Appl*. *Phys*. *Lett*. **100** 212108

[23]. Nayak P K, Hedhili M N, Cha D and Alshareef H N 2013 *Appl*. *Phys*. *Lett*. **103** 033518

[24]. Lei F, Sun Y, Liu K, Gao S, Liang L, Pan B and Xie Y 2014 *J*. *Am*. *Chem*. *Soc*. **136** 6826

[25]. Shanmugasundaram A, Ramireddy B, Basak P, Manorama S V and Srinath S 2014 *J*. *Phys*. *Chem*. *C* **118** 6909

[26]. Yoo Y K, Xue Q, Lee H C, Cheng S, Xiang X D, Dionne G F, Xu S, He J, Chu Y S, Preite S D, Lofl S E and Takeuchi I 2005 *Appl*. *Phys*. *Lett*. **86** 042506

[27]. Feng Q, Blythe H J, Jiang F X, Xu X H, Heald S M, Fox A M and Gehring G A 2013 *APL Mater*. **1** 022107

[28]. Jahangir S, Dogan F, Kum H, Manchon A and Bhattacharya P 2012 *Phys*. *Rev*. *B* **86**

035315

[29]. Kum H, Heo J, Jahangir S, Banerjee A, Guo W and Bhattacharya P 2012 *Appl. Phys. Lett.* **100** 182407

[30]. Yu Z, He J, Xu S, Xue Q, van't Erve O, Jonker B, Marcus M, Yoo Y, Cheng S and Xiang X D 2006 *Phys. Rev. B* **74** 165321

[31]. Wang X F, Song F Q, Chen J, Wang T Y, Wang J L, Liu P, Shen M R. Wan J G, Wang G H, and Xu J B 2010 *J. Am. Chem. Soc.* **132** 6492

[32]. Zou C W, Wu H Z, Liang F, Xue S W and Shao L X 2014 *Appl. Phys. Lett.* **104** 222105

[33]. Farvid S S, Sabergharesou T, Hutfluss L N, Hegde M, Prouzet E and Radovanovic P V 2014 *J. Am. Chem. Soc.* **136** 7669

[34]. Wang X F, Wan B, Zhang K, Zhao B, Li Z, Wan X, Song F Q, Liu B, Xiu X Q, Xu Y B, Shi Y and Zhang R 2013 *J. Phys. Chem. C* **117** 18258

[35]. Wang X F, Zheng R K, Liu Z W, Ho H P, Xu J B and Ringer S P 2008 *Nanotechnology* **19** 455702

[36]. Koo B R, Park I K and Ahn H J 2014 *J. Alloy. Compd.* **603** 52

[37]. Meng X Q, and Li J B 2010 *J. Phys. Chem. C* **114** 17569

[38]. Yin W Y, Cao M H, Ni C Y, Cloutier S G, Huang Z G, Ma X, Ren L, Hu C W, and Wei B Q 2009 *J. Phys. Chem. C* **113** 19493

[39]. Singhal S N A, Manjanna J, Jayakumar O D, Kadam R M, and Tyagi A K 2009 *J. Phys. Chem. C* **113** 3600

[40]. Xing P F, Chen Y X, Yan S S, Liu G L, Mei L M and Zhang Z 2009 *J. Appl. Phys.* **106** 043909

[41]. Guan L, Tao J, Xiao Z, Zhao B, Fan X, Huan C, Kuo J and Wang L 2009 *Phys. Rev. B*

79 184412

[42]. An Y, Wang S, Feng D, Wu Z and Liu J 2013 *Appl. Surf. Sci.* **276** 535

Figures

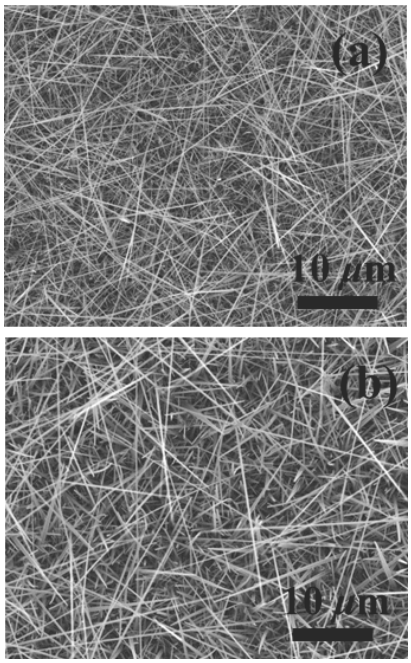

Fig. 1 Typical SEM images of (a) pure In_2O_3 and (b) Fe-doped In_2O_3 nanowires.

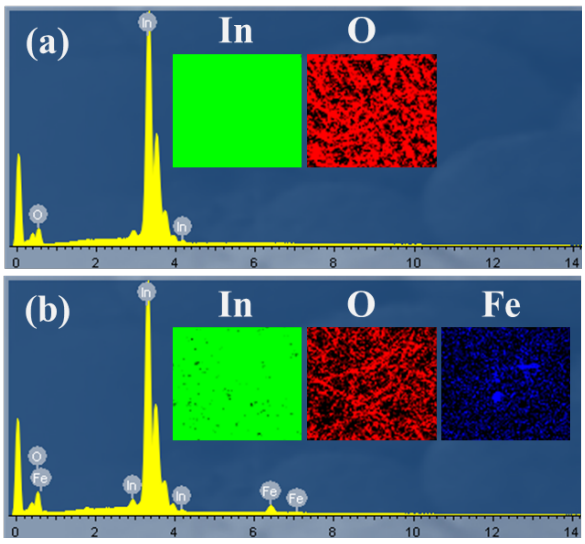

Fig. 2 EDS spectra of (a) pure In_2O_3 and (b) Fe-doped In_2O_3 nanowires, insets are elemental mapping of In, O, and Fe in pure In_2O_3 and Fe-doped In_2O_3 nanowires, respectively.

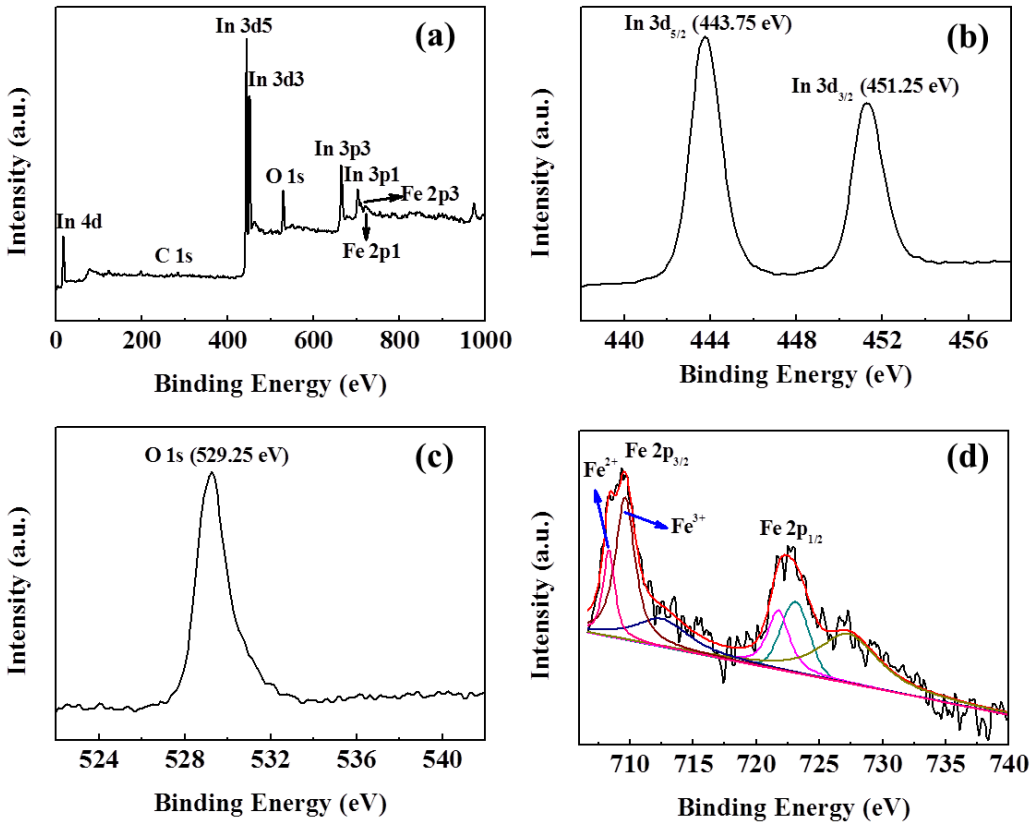

Fig. 3 (a) XPS survey spectrum of Fe-In_2O_3 nanowires, (b-d) high-resolution XPS spectra of In 3d, O 1s, and Fe 2p, respectively. The peaks in (d) are divided by Gaussian peak-fitting.

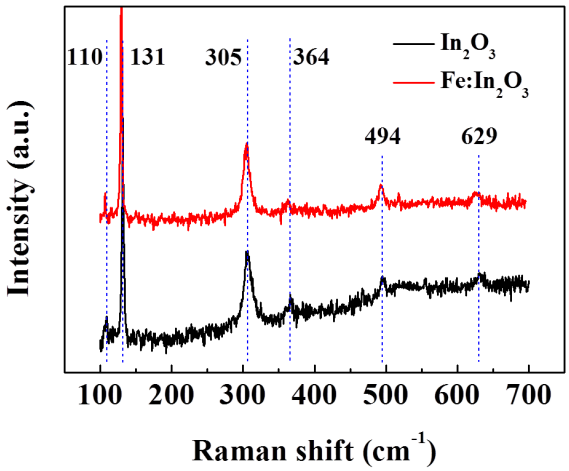

Fig. 4 Room temperature Raman spectra of pure In_2O_3 and Fe-doped In_2O_3 nanowires.

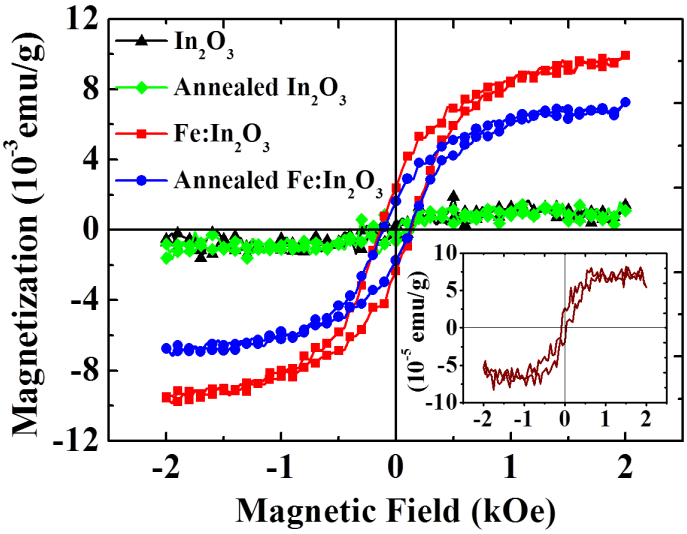

Fig. 5 Magnetization as a function of magnetic field at room temperature for In_2O_3 and Fe-doped In_2O_3 nanowires before and after annealing. The inset shows magnetic hysteresis loop of substrate without nanowires.